Brandon Research, Inc. Orthopedic Implant

Cooperative Research and Development Agreement (CRADA) Final Report

Federal Manufacturing & Technologies

W. R. Freeman

KCP−613−6133

Published April 1999

Final Report

CRADA Number KCP−94−1003

AlliedSignal

Prepared Under Contract Number DE−ACO4−76−DP00613 for the

United States Department of Energy

DISCLAIMER

Printed in the United States of America.

This report has been reproduced from the best available copy.

Available to DOE and DOE contractors from the Office of Scientific and Technical Information,
P. O. Box 62, Oak Ridge, Tennessee 37831; prices available from (423) 576−8401,
FTS 626−8401.

Available to the public from the National Technical Information Service, U. S. Department of Commerce,
5285 Port Royal Rd., Springfield, Virginia 22161, (703) 487−4650.

AlliedSignal Inc.

Federal Manufacturing
& Technologies

P. O. Box 419159

Kansas City, Missouri

64141−6159

A prime contractor with the United States

Department of Energy under Contract Number

DE−ACO4−76−DP00613.

KCP−613−6133

Distribution Category UC−706

BRANDON RESEARCH, INC. ORTHOPEDIC IMPLANT

COOPERATIVE RESEARCH AND DEVELOPMENT AGREEMENT (CRADA) FINAL REPORT

W. R. Freeman

Published April 1999

Final Report

CRADA Number KCP−613−1003

Contents

Section

Abstract

Summary

Discussion

Scope and Purpose

Activity

Technical

Assumptions and Limitations of Simulations

Results of Simulations

Partner Contribution

Financial

Property and Proprietary Information

Acknowledgment

References

Bibliography

Illustrations

Figure

1a Shaded image of finite element model of left femur, anterior

1b Shaded image of finite element model, posterior

1c Shaded image of finite element model, medial

2a Overall view of finite element model, intact femur

2b Proximal detail of finite model, intact femur

3 Section view of implant located in prepared femur, without cement

4a Finite element model of femur after total hip arthroplasty

4b Proximal end details of FE model

5 Finite element model of implant device

6 Contour plot of Von Mises strain on exterior surface of intact femur

7 Contour plot of Von Mises strain on exterior surface of implanted femur−−with cobalt−chromium implant

8 Contour plot of Von Mises strain with titanium implant

9 Contour plot of Von Mises strain with aluminum implant

10 Contour plot of Von Mises strain with bone modulus implant

11 Strain plot on proximal end of femur with cobalt−chromium implant

12 Strain plot on proximal end of femur with titanium implant

13 Strain plot on proximal end of femur with aluminum implant

14 Strain plot on proximal end of femur with bone modulus implant

15 Strain plot on longitudinal cutting plane through intact proximal femur

16 Strain plot on longitudinal plane cut through proximal femur, cobalt−chromium implant

17 Strain plot on longitudinal plane cut through proximal femur, titanium implant

18 Strain plot on longitudinal plane cut through proximal femur, aluminum implant

19 Strain plot on longitudinal plane cut through proximal femur, bone modulus implant

20 Strain plots on sections of intact femur

21 Strain plots on sections of femur, with cobalt−chromium implant

22 Strain plots on sections of femur, with titanium implant

23 Strain plots on sections of femur, with aluminum implant

24 Strain plots on sections of femur, with bone modulus implant

25 Strain plots on longitudinal section through proximal femur, high modulus cement with cobalt−chromium implant

26 Strain plots on longitudinal section through proximal femur, standard cement with cobalt−chromium implant

27 Strain plots on longitudinal section through proximal femur, low modulus cement with cobalt−chromium implant

Tables

Number

1 Materials Used in Comparative Hip Implant Finite Element Analyses

2 Load Case Definition

3 Maximum Strain on Medial Surface of Proximal Femur for Different Implant Materials

4 Maximum Strain for Different Implant Materials on Anterior Surface of Proximal Femur Approximately 10 mm Perpendicular to Angled Preparation Cut

5 Maximum Strain for Different Implant Materials on Longitudinal Section of Proximal Femur on Surface of Interior Preparation Cut

6 Comparison of Effects on Strain Distribution of Cement Stiffness Changes

Abstract

The project was a joint research effort between the U. S. Department of Energy s (DOE) Kansas City Plant (KCP) and Brandon Research, Inc. to develop ways to improve implants used for orthopedic surgery for joint replacement. The primary product produced by this study is design information, which may be used to develop implants that will improve long−term fixation and durability in the host bone environment.

Summary

There are approximately one million hip, knee, and shoulder implants per year worldwide. Unfortunately, the typical lifetime of these implants is ten years. This project was established because significant improvements are needed in implant design to extend their useful lifetime. An important issue in joint arthroplasty is bone resorption. In bone resorption, the bone actually remodels its internal structure in adapting to changes in the bone strain state caused by the implant, causing bone to disappear. Implant−induced bone resorption and implant wear are the two primary concerns in orthopedic surgery today. By combining the Kansas City Plant's (KCP s) finite element structural analysis capabilities and Brandon Research s technical and medical expertise, improved understanding of the effects of implant designs can be developed to better deal with implant−induced bone resorption. The improvements developed in this project will contribute to

- minimize or avoid bone loss,
- extend the useful life of the implant,
- postpone or avoid implant replacement,
- improve the quality of life for the 500,000 annual U.S. implant patients.

KCP s integrated solid modeling and advanced finite element stress analysis was coupled with the design, geometry, loading, and material property data from experienced medical researchers to provide accurate, detailed analysis to study advances in implant design which are not available otherwise. Previously reported work has been limited to relatively coarse models, probably due to software and computer hardware limitations.

This project utilized actual bone geometric shape data from Computerized Axial Tomography (CAT) scans linked to a medical CAD system. The geometric information was transferred to KCP s integrated solid modeler and finite element preprocessor to produce more detailed and accurate finite element models of bone and implant than models used in previously reported work. These improved models were used to simulate the performance of existing design and modified implants. These simulations provided accurate, high−resolution color strain plots for both the implant and the surrounding bone. The availability of the KCP Cray supercomputers was a key factor which dramatically expanded the model geometric accuracy and the limits of strain resolution compared to previous work reported in the field.

KCP s decades of finite element analysis experience, world−class software, and supercomputer hardware, combined with the knowledge and experience of the team s orthopedic surgeons and implant experts, have provided results which contribute new information which can be used to improve the implant−induced strain distribution. Improved strain distribution is expected to increase implant life, which would represent a

significant benefit to patients and society as a whole.

This team has leveraged the existing Department of Energy (DOE) technology base, along with medical and business experts in the orthopedic implant field, to verify in a thorough and methodical simulation study that reduced implant stiffness causes more uniform and greater magnitude strain in the proximal femur. Current understanding of the process of bone remodeling in response to strain indicates that more uniform and greater magnitude strain in the proximal femur should lead to improvements in orthopedic implant long−term functionality because of reduced bone resorption in the proximal femur.

The simulation results indicate that total hip arthroplasty (replacement of the proximal femoral head with an implant) inherently changes the strain distribution in the femur. Reduced stiffness with this particular implant geometric design cannot restore the strain distribution to the strain distribution of an intact femur. Reduction in stiffness of the implant redistributes the strain more uniformly throughout the proximal femur and increases the maximum strain in the proximal femur. Both of these effects are expected to be beneficial.

The length of the implant stem is a significant factor controlling the strain distribution after total hip arthroplasty. In the intact femur, the strain shifts from compressive on the medial interior surface of the femur to compressive on the exterior surface approximately 125 mm from the top of the greater trochanter. After total hip arthroplasty, the strain inflection point is displaced to beyond the tip of the implant, approximately 215 mm from the top of the greater trochanter. This inflection location does not change location significantly with reduced implant stiffness. The simulations verify that strain in the proximal femur increases due to modifying hip implants to reduce stiffness.

Discussion

Scope and Purpose

The initial plan was to transfer the CAT scan derived medical computer aided design (CAD) system surface model of a human femur to the engineering solid modeling and finite element modeling system. Once the intact human femur was converted to a solid model in the receiving modeling system, a finite element model would be analyzed to produce the baseline strain distribution in an intact human femur. After the intact femur study was completed, the femur model would be modified to include the hip implant, which would create a model of the femur after total hip arthroplasty. The goal was to modify the implant to produce a strain distribution in the femur after total hip arthroplasty that is more like the strain distribution in the intact femur than standard designs.

Activity

Technical

Modeling

Within a few days of the beginning of the technical work, technical problems were discovered that eventually would require far more time to solve than was originally planned. The intact femur model received from the medical CAD (computer aided drafting) system appeared to import into the CAE (computer aided

engineering) solid modeling system as a pair of valid surfaces, but the engineering solid modeling system was unable to do any subsequent operations on these surfaces. Exhaustive analysis of the surfaces discovered a very small, mathematically possible but ambiguous, nonsensical condition where a portion of the surface locally loops around itself. This mathematical ambiguity is an artifact of the medical CAD surface creation methodology, which randomly generates such flaws. This ambiguous surface loop prevented any subsequent operations with this mathematically flawed surface of the intact femur. Tests showed that all such medical CAD system−generated surfaces had such flaws, and this particular model had much fewer than the average number of flaws. The medical CAD system could deal with these flaws internally without problems, so there was no method for preventing or removing them in the originating software system. Methods were developed in the engineering solid modeling system to remove this ambiguous region and replace it with a surface that retained the connection to the original femur geometry yet eliminated the local loop in the surface.

This "repair" left the outer surface of the femur solid model in several portions, some created directly from the original medical CAD system, and some re−created within the engineering solid modeling system. This mixing of geometry caused additional difficulties in the receiving solid modeling system. It became necessary to "clean up" portions of the imported geometry

and rebuild the surfaces from these portions. Further work found that the medical CAD CAT−scan data conversion process also introduced serious distortion of the surfaces on the underlying parametric level. While these surfaces appear perfectly acceptable in normal Cartesian space, they had severe distortions in their parametric space descriptions, which resulted in unacceptable distortion of the elements when finite element modeling was attempted. These inherited parametric distortions had to be "cleaned" from the model before any subsequent operations would yield useful results. This was a very time−consuming and difficult process which had not been predicted.

One of the great learning experiences in this project involved reaching, exceeding, and understanding, and ultimately working within, the limitations of an engineering−oriented solid modeling system in dealing with bio−shapes. The lack of defined edges on bio−shapes to delimit surfaces is dramatically different than the usual multi−surfaced man−made shapes used in engineering. The inability of the engineering system to deal effectively with "poles," where all the parametric lines which define the surface have a common point, required the development of alternate methods, which was a major technical difficulty and took considerable effort to overcome. These poles are much like the longitude lines on earth joining at the north and south poles. Another fundamental limitation in some engineering−oriented solid modelers is the difficulty of joining lofted surfaces along edges while maintaining tangency of the surfaces at all locations along the joint. This stringent tangency is not usually necessary for engineered objects since they have edges and corners, yet is the norm for bio−shapes which typically blend smoothly from one surface to the adjacent surface. As these individual incompatibilities in solid modeling concepts between medical/bio systems and engineering systems were discovered, work−arounds were carefully developed. All these educational opportunities consumed more time than was originally planned in the model conversion and creation phase.

Eventually, a valid solid model of the intact human femur was created and converted to a high−resolution finite element model. The finite element model is presented as shaded images in Figure 1a−c and line plots show the element size and density in Figures 2a and 2b. (Figures appear following the text.) This model consisted of 67,649 second−order tetrahedron elements, which have ten nodes per element. The model was analyzed successfully with ABAQUS/Standard finite element analysis software, using the same loading condition as would be used for the implanted femur.

The project moved to the next phase, which was to import the CAD model of the hip implant device and incorporate it into a model of total hip arthroplasty with a cemented implant device. This geometry importation went reasonably well and the solid model in the receiving mechanical CAD system was made with a moderate level of manual "fix−up." This sort of manual fix−up is usually necessary because of

functional incompatibilities between engineering solid modeling systems from different manufacturers.

The implant was scaled to fit the particular human femur used for this study. Implant size and location were directed and approved by the Brandon Research doctors. The particular implant used is a cemented design, which requires a clearance of three to five millimeters all around the implant for the cement to bond the implant into the femoral cavity.

Total hip arthroplasty requires the removal of the original femoral head and drilling into the proximal end of the femur under the original head to open a cavity which joins the existing internal femur cavity. These cuts and the bone removal to open access into the existing internal cavity were complex to align so that the final implant position would be within the resulting void, with a consistent clearance all around for the cement. See Figure 3 for an image of the implant device located in the prepared femur, without cement shown.

Once the femur solid model was prepared by removing the head and opening an access hole to the femoral canal, a cement solid model was created which matched the interior of the prepared femur and the exterior of the implant device. This was accomplished with Boolean cutting operations, ensuring precise fitting of the cement between the implant and the femur.

At this point, the solid model creation process seemed to be going well. Expectations were that the process would directly produce a valid finite element model with three defined volumes: the femur, the cement, and the implant. Unfortunately, there was no success at converting the three apparently valid solid volumes into a valid finite element model. Although no definitive explanation for the meshing failure was ever developed, the most likely cause is the accumulated small errors caused by complex mixed−source geometry. The stability of non−native geometry in advanced solid modeling systems is always in question due to the difficulty of converting the non−native geometry into the native system without errors. The technical challenge in developing mathematically rigorous software tools for complex solid modeling operations is very difficult, even with total control of the geometric model creation process and the underlying database. When the creation process and database are compromised by translation of geometry from a foreign system, the results are sometimes unpredictable and inconsistent. This is not a condemnation of the software, but an acknowledgment of the subtle and critical nature of solid modeling data. It would be very useful if this sort of translation were deterministic and always resulted in a solid model which was as valid and as stable as a native model. This certainty of conversion between dissimilar systems is not available at the current level of development of solid modeling software.

The necessary element creation was far too complex for manual element creation (meshing) methods, and the automated methods had failed. It appeared that the project would not be successful, primarily due to solid model data conversion between dissimilar systems, which had been a severe problem from the beginning.

After many months of attempting various subtle and finely detailed methods to improve the quality and stability of the solid model enough to produce a valid finite element model, a new release of the solid modeling software presented a new capability which proved to be the key to the ultimate success of the project.

This new capability was specifically intended to deal with some of the problems involved in finite element modeling based on imported (non−native system) geometry, which was the problem that was stopping progress in this project. This new software feature provided the capability to create solid finite elements to fill any volume defined by a valid fully closed set of surface (shell) finite elements. The advantage was that surface meshes of shell finite elements are mathematically dramatically simpler than solid models, so there is less likelihood of subtle inconsistencies with a surface mesh. Even more importantly, if there are problems with a surface mesh, it is relatively easy to manually "repair" small problems along the edges of adjacent surface meshes to ensure closure. Repair of incompatible surface meshes is possible because the user has

direct control of the nodes and elements that define the surface mesh. This user control is unavailable in the solid modeling function. This new software tool was a major breakthrough for the project.

A valid, accurate finite element model of each of the three components of the total hip arthroplasty model−−the femur, the cement, and the implant−−were created separately via the surface meshing method. These models were joined after creation. This process created objects that were not linked in any analytical sense and would therefore not interact. Since this interaction was the crux of the project, this required correction. The only way for these three solids to be joined in the final finite element model was to use the *same* surface mesh (nodes and elements) for coincident (yet different) surfaces that would later be joined. For example, the surface mesh that defined the *interior* of the femur was also used to define the *exterio*r of the cement, a shared surface. This ensured absolutely identical location of nodes and definition of elements on this common surface between the femur interior and the cement. Later, the coincident nodes (one set from the femur interior and an identically locate set from the cement exterior) could be joined with standard finite element model cleanup tools which remove coincident nodes and connect the elements. This resulted in linking the cement exterior to the femur interior perfectly.

This same method was used so that the implant exterior surface and the cement interior surfaces were created with the same surface mesh, ensuring perfect compatibility when they were later joined. This process was more time−consuming than fully automatic methods, but since the fully automatic methods were not working, it was a welcomed capability.

Finally, a geometrically relatively accurate and detailed finite element model was created simulating a human femur with total hip arthroplasty using a cemented implant, ready for analysis and results comparison to the intact human femur. See Figures 4a and 4b. This model had 59,991 second−order tetrahedron elements.

The Brandon Research orthopedic surgeons selected the particular implant device that was modeled for this study because it is a widely used implant, and there is much field data on the effect of long−term implantation. The implant finite element model is shown in Figure 5.

The primary purpose of this research project was to improve the durability of implants by changes that would improve the strain distribution in the implanted femur to more closely match the strain distribution in the intact femur. Reading other research studies of this problem led to understanding the concept of the implant "stealing strain" from the surrounding bone, which leads to bone resorption. Since the strain in the implant is inversely proportional to the stiffness of the implant, increasing the strain in the surrounding bone would require reducing the strain in the implant, implying a reduction in stiffness in the implant. There are two components that contribute to the stiffness of the implant that are controllable and that could be modified to reduce the implant stiffness. The first component of implant stiffness is the geometry of the implant, and the second is the modulus of elasticity of the implant material. Implant material properties were selected as the method of implant stiffness variation because of the considerable difficulty of modifying the implant geometry and the ease of modifying the implant material properties. Examination of the effects of variation in geometry to modify the stiffness distribution in the implant will have to wait for another research project. This study examined varying the overall stiffness *level* but leaving the stiffness *distribution* (which is controlled by the geometry of the implant) the same.

The modulus of elasticity, or Young s modulus, is different for different materials. Table 1 gives examples of the Young s modulus for the materials that were chosen for this study.

Table 1. Materials Used in Comparative Hip Implant Finite Element Analyses

Material	Young s modulus
Cobalt−chromium−moly alloy	2.14E+5 MPa
Titanium 6Al−4 V alloy	1.14E+5 MPa
Aluminum 2024 alloy	7.31E+4 MPa
Bone modulus material − a nonspecific glass/polymer composite	1.40E+4 MPa
Acrylic cement	2.30E+3 MPa

As previously stated, the geometry of the implant was not varied during this study. To vary the stiffness of the implant, the modulus of elasticity was varied, using the materials shown in Table 1. The first material, the cobalt−chromium−moly alloy, was included in the study because it is the material currently used to make the particular implant device studied.

Titanium alloy was selected for study for two reasons. First, titanium alloy has been used for bioimplants and is, therefore, a standard material that is acceptable for implants. Second, titanium is approximately half as stiff as the cobalt−chromium−moly alloy, which is a convenient change in stiffness value to evaluate. The third material studied was aluminum alloy.

Aluminum has no known history of use in bioimplants, and may prove unsuitable in an unprotected form for long−term service inside the human body, due to corrosion. However, aluminum is a normal structural material which is capable of supporting the necessary loads if properly designed, and aluminum has a Young s modulus which makes it about one−third as stiff as the cobalt−chromium−moly alloy, which is also a convenient increment in stiffness. If an aluminum alloy were to be used in the human body, there are various ways to plate or coat an aluminum alloy implant to improve the corrosion resistance that may prove acceptable for bioimplants. At this stage, the primary point is to examine the structural effects of various available materials for possible use in implant devices. Biocompatibility questions can be dealt with later, if the material shows promise for structural reasons.

The last material selected is not a specific material, but just a substance with a set of material properties that are similar to cortical bone. There are actual materials (such as glass−filled polymers) which have Young s modulii similar to the values used, so if this class of materials proves to be structurally advantageous, an actual material could be selected from the possible choices and tested for biocompatibility, manufacturability, and other requirements for an implant material. The point here is to evaluate whether there are structural advantages to using a low modulus material for implants.

The other material property that was varied was the stiffness of the cement used to fix the implant to the

femur. No attempt was made to select actual materials for the increased and decreased stiffness cement cases. This was because the primary point was to study the effect of modified cement stiffness on strain distribution in the femur, rather than study a particular cement material. The cement used in all the models that have variable implant stiffness was the typical acrylic cement, with a Young s modulus of about 2,300 MPa.

In order to study the effects of both higher stiffness and lower stiffness cements, two models were run using the standard cobalt−chromium−moly alloy implant and the two modified cements. The two "new" cements studied represented materials with ten times the stiffness and one−tenth the stiffness of the standard acrylic cement. This range of cement stiffness was selected because it represents a large enough change in cement stiffness to cause the effects of cement stiffness to be apparent. If the effects on femur strain distribution proved to be very small with an order of magnitude change in cement stiffness, then it would be clear that small changes in cement stiffness are relatively unimportant.

It would have been possible to have studied the effects of increasing or decreasing the cement stiffness by a factor of 10 with each of the different implant materials. This would have generated a much larger quantity of data, and time did not permit a fully exhaustive evaluation of this type. The results of the cement modulus variation may suggest that further study would be useful, but a full examination of cement modulus variation along with implant modulus variation is beyond this study.

Assumptions and Limitations of Simulations

The simulations carried out as a part of this study were done within the limitations of time and effort that all such studies have to contend with. In addition, there are limitations to the software tools and the available computer hardware to solve the problems.

This sort of study cannot include all possible effects as a part of the model, so certain simplifying assumptions are required. It is best to specifically catalog these assumptions and limitations to the model(s) and to point out the possible effects that these assumptions and limitations might have on the results. This sort of candor is necessary to ensure that the study results are understood in the proper context. Explicit statement of limitations ensures that the reader understands what is included in the models and does not assume the model to include some effects or features that were not, in fact, included in the model. The authors would suggest that there are important benefits to explicit reporting of assumptions and limitations when dealing with simulations, and they should always be clearly presented in a final report.

Bone Material Properties

One of the primary limitations to this study is the material properties used for the bone. Multiple sources were consulted and various material properties were found in the literature. Unfortunately, biomaterials are not as simple as man−made structural metal alloys. While steel may vary somewhat from lot to lot, it has properties that are generally very close to the published material properties. Metals also have the advantage of being isotropic, which permits mechanical response to be described mathematically with only two independent variables: modulus of elasticity and Poisson s ratio. Bone is highly non−isotropic, has large density and modulus variations both by location and by direction. Several authors of biostructural studies published in the literature (Carter[1] and St. Ville[2]) have specified various mathematical relationships between the density of bone and it s Young s modulus. Even when reported, there is discussion whether the exponent of the proposed density−stiffness relationship is closer to 2 or 3. In addition, different sources provide widely varying values for Young s modulus for both cortical and cancellous bone. Even the

terminology "cortical" and "cancellous" are inadequate to accurately describe a material which exists on a continuum from the highest density cortical bone to the lowest density cancellous bone, with material properties that vary by more than an order of magnitude. No doubt a substantial part of the difficulty is the normal biological variability from individual to individual in bone structural properties, which are probably affected by diet, activity level, heredity, and lifestyle choices.

In some previously published research studies, an effort has been made to assign material properties to elements based on the apparent density in a particular example bone which was studied in detail and modeled with variable material properties. Given that these previously reported studies have typically used very coarse meshing (physically large individual finite elements), there is certain to be substantial variation of density and thereby material properties within any particular element that must be ignored to assign an average property to the element. Without disagreeing that this effort to vary bone properties within the model may be a viable and probably beneficial approach, this study made no such attempt to approximate the local variation in bone material properties.

The material properties of bone are also nonisotropic, but not necessarily orthotropic, since the natural growth of bone has primary strength directions which are apparently loading−based and do not respect the Cartesian coordinate system s mathematically convenient mutual perpendicularity. Properly describing a fully non−isotropic material can require up to 36 terms in the material matrix. Many of these material properties are extremely difficult to accurately measure in the laboratory, even with man−made relatively homogeneous materials. An exhaustive characterization of the material properties of human bone was beyond the scope of this project.

It is little or no exaggeration to say that it is unlikely that we will ever have a highly accurate material model for human bone. There is no question that bone material models will improve and will eventually be capable of accounting for much more of the material phenomena than are accountable today. However, the science of bone material properties is immature and the data is, to date, fragmentary and, to some degree, contradictory. So, extreme precision in bone material properties does not appear to actually be possible. Ultimately, the variability of bone morphology and structural properties in the actual human population limits the applicability of mechanical strain and stress studies like this to a moderate level of precision at best.

Given the current limitations of scientific knowledge on the material properties of bone, this project chose to partially sidestep the bone material properties issue by using the average value for cortical bone from several sources. One of the factors that mediates for this approach is that the majority of the bone remaining in the proximal femur after the preparation for total hip arthroplasty has been completed is cortical bone. The comparisons made in this report primarily deal with comparing one implanted femur to another with identical geometry, but different implant or cement materials. The lack of cancellous bone material properties in the models used in this report will primarily affect the stresses in the intact femur model, particularly in the femoral head which has substantial cancellous bone in the interior. Since much of this cancellous bone is removed in the implant preparation process, there is no direct comparison possible (or necessary) for the portion of the femur where the error due to simplified material properties is the greatest, the femoral head and neck. The approach used in this report does not claim to yield the ultimate solution to the bone material property problem, but it is a particular simplifying assumption that makes it possible to move ahead and deal with the real topic, which can be controlled and accurately defined; implant stiffness.

Loading Condition

The Brandon Research medical staff selected the loading condition used. It is based on loads used in a research project reported by Carter in 1989.[1] This load represents the single−limb−stance phase of gait. The

load applied was divided into two regions, the femoral ball and the greater trochanter where the hip abductor loads are applied. Converting the Carter report loading to the coordinate system used in this model and converting the vectors resulted in the following loading condition, presented as Table 2 and the adjacent figure.

Table 2. Load Case Definition

Location	Carter Case 1 Total Load	Angle From Femur Long Axis	Femur Long Axis Component	Perpendicular Component
Head	2317 N	24^o	2117 N	−942 N
Abductor	702 N	28^o	−620 N	330 N

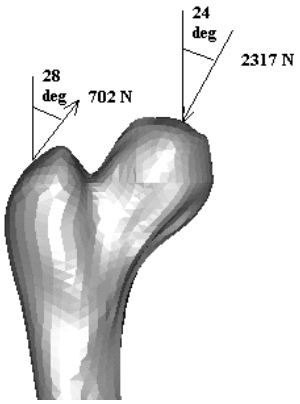

This is a commonly used loading condition, although various authors make slightly different assumptions of load magnitude and application directions. This is a static load, where the actual walking load is continuously varying dynamic load, which changes direction and magnitude rapidly during gait. This load is a representative example of the higher portion of the loading during gait and is a valid static example.

Support Condition

The support condition is the other boundary condition required to constrain the femur model from rigid body motion. Since the support of the femur comes from the distal end during gait, the support condition was logically applied at the distal surface. Nodes on an appropriate portion of the surface of the condyles were constrained rigidly in place. This is likely to provide a somewhat different strain distribution near the support locations (condyles surfaces) than might be measured in a living femur, but at locations a short distance away from this simplified support condition the accuracy of the strain distribution will quickly approach the correct distribution. Essentially all boundary conditions are necessarily simplified approximations of real loading and support conditions, and it should always be kept in mind that strain and stress values very near any boundary conditions are highly suspect. This is the primary reason to avoid using a femur model that does not model all

the way to the condyles.

Implant Contact

The implant used in this study has a pair of planar surfaces where the head/neck section transitions to the stem section. These planar ledges contact the planar surface of the angled preparation cut in the femur. In this series of models, the implant was considered to be bonded to the femoral surface at all points of contact, including this planar area (prep cut) which may have questionable bonding in actual practice. In general, the strains reported were small in the areas where tensile forces may be developed between this particular implant surface and the bone due to the applied loads. This low tensile strain indicates that adding contact elements to this region to prevent development of inappropriate tensile forces would be unlikely to significantly affect the results. This would be a possible area to test future improvement to the models.

Results of Simulations

Overview

The simulation results indicate that total hip arthroplasty fundamentally alters the strain distribution in the femur. This should not be surprising. These simulations make it clear that

- Reduction in stiffness with current implant geometry redistributes the strain more uniformly throughout the proximal femur and increases the maximum strain in the proximal femur.
- Reduced stiffness with current implant geometry cannot restore the strain distribution in the femur after total hip arthroplasty to the strain distribution of an intact femur.
- The length of the implant stem is a major factor affecting the strain distribution after total hip arthroplasty. Even with a low modulus implant, the strain inflection in the femur was displaced nearly 100 mm to beyond the stem tip.
- Changing cement stiffness modifies local strains near the implant flange. Stiffer cement produces higher local strains; more flexible cement produces lower local strains.
- Changing cement stiffness modifies the overall strains in the femoral shaft. Stiffer cement produces lower shaft strains; more flexible cement produces higher shaft strains.

In the intact femur, for the particular load used, the strain shifts from compressive on the medial surface of the femur to compressive on the lateral surface approximately 125 mm from the tip of the greater trochanter. After total hip arthroplasty, the strain inflection point is displaced to beyond the tip of the implant, approximately 215 mm from the tip of the greater trochanter. This strain inflection does not change location significantly with reduced implant stiffness.

The simulations verify that strain in the proximal femur increases when the stiffness of a hip implant is reduced. The simulations have demonstrated that reduced implant stiffness can increase the local strain in some regions by as much as 94%.

Cement stiffness significantly shifts the strain distribution in the proximal femur when used with a relatively

stiff implant made of cobalt−chromium alloy. Higher modulus cement causes the local strains at the proximal end of the femur (near the implant flange) to increase and the compressive strains in the proximal 150 mm of the shaft strains to decrease. Lower modulus cement reduces the local strains at the proximal end (near the implant flange) and increases the compressive strains in the proximal 150 mm of the femoral shaft.

Details of the Simulation Results

Color plots of the surface strains on the whole femur, both intact and with different stiffness implants are presented in Figures 6 through 10. Figure 6 is the intact femur, and is the reference strain state to which the implanted femur will be compared.

A longitudinal section plane through the femur was defined by locating two points in the approximate center of the femoral canal, near the distal and proximal ends of the canal. The third point was located at the approximate center of the spherical head of the implant. The plane defined by these three points is oriented to pass through the approximate center of the femur over the entire length, but due to the curvature of the femur along the long axis, the plane is somewhat off the shaft center near the middle of the femur. This plane is not well located for examining the strains inside the implant device, since the implant is oriented relative to the upper portion of the femoral preparation cut, rather than to the overall femoral canal.

A series of cross−section planes was defined perpendicular to the long axis of the femur, as defined by the approximate centers of the proximal and distal portions of the femoral cavity. These cross−section planes were located at 20−mm intervals, and strain plots were made for these sets of cross sections.

The intact femur had significantly lower maximum strains in the proximal region than did any of the cases with an implant device. Even the lowest stiffness implant substantially changed the strain distribution in the proximal femur. Since a significant amount of interior bone is removed to create the prepared channel for the implant stem, the implant and the remaining bone carry the strain. As the implant stiffness is reduced, the strain increases in the bone of the proximal femur, so that the proximal femoral bone is subjected to a significantly higher strain in some regions after total hip arthroplasty compared to the intact femur. The highest local strains are located where the flange on the implant device mates against the preparation cut. The lower portion of this flange causes very high local compressive strains in the femur. Figures 11 though 14 show the local high strain regions adjacent to the bone that was removed from the proximal femur for access to the canal for the implant device stem. In these strain plots, the peak strain in this local area is higher than the maximum value on the color bar (legend). This results in the plotting software leaving the higher strain areas out of the plot, which is visible in the figures as a black region.

Other parts of the femur are subjected to very low strains after total hip arthroplasty. For the load condition used in this study, the entire greater trochanter is subjected to very low strains, both in the intact femur and after arthroplasty.

In addition to the change in magnitude of the maximum strains in the proximal femur, the strain distribution is significantly affected by both the bone removed in preparation for the implant and the presence of the implant. The load case used for this study causes the femur to deform slightly into an "S" shape, due to the applied moment at the femoral head area. The inflection point, located where the compressive stresses drop to zero and then become tensile stresses (like the center of the S) is shifted distally by the presence of the implant. The inflection point is shifted to just beyond the tip of the implant in all cases. This is due to the localized stiffening of the proximal femur by the implant. Even the most flexible implant caused the point of inflection to move distally to the location of the implant tip.

In the intact femur, for the particular load used, the strain shifts from compressive on the medial surface of

the femur to compressive on the lateral surface approximately 125 mm from the top of the greater trochanter. After total hip arthroplasty, the strain inflection point is displaced to beyond the tip of the implant, approximately 215 mm from the top of the greater trochanter. This strain inflection does not change location significantly with reduced implant stiffness.

It seems reasonable that a shortened implant stem would reduce this effect, but this was not simulated. Refer to Figures 6 through 10.

The results of the simulations indicate very clearly that the reduced stiffness implants increased the strain in the proximal femur. In effect, the implant "steals strain" from the bone, so a more flexible implant shifts more of the strain to the bone. This is very clear from a comparison of Figures 11 through 14, which represent a set of pairs of color contour plots of Von Mises strain on the surface of the prepared proximal femur.

The peak strain on the surface for the standard cobalt−chromium alloy implant (Figure 11) is located approximately 40 mm from the edge of the preparation cut. The peak surface strain at this point is shown in Table 3 for this location on the medial surface of the proximal femur.

Table 3. Maximum Strain on Medial Surface of Proximal Femur for Different Implant Materials

Implant Material	Max Strain, at Medial Surface of Proximal Femur	Change in Strain Relative to Co−Cr	Specific Modulus Relative to Co−Cr
cobalt−chromium	1.17E−3	baseline	1.0
titanium	1.44E−3	+23%	0.53
aluminum	1.55E−3	+32%	0.34
bone modulus	1.83E−3	+56%	0.07

For these cases, the location of the maximum strain on the surface remains essentially the same, but increases in magnitude as the implant modulus decreases. Clearly, reduced implant stiffness has a substantial effect, increasing the surface strain in the proximal femur by up to 56%, even though the geometry of the implant is unchanged.

Looking at the anterior surface of the proximal femur approximately 10 mm along the surface perpendicular to the angled preparation cut, there is a local maximum strain. A comparison of the strains in this location for different implant materials is presented in Table 4.

Table 4. Maximum Strain for Different Implant Materials on Anterior Surface of Proximal Femur Approximately 10 mm Perpendicular to Angled Preparation Cut

Implant Material	Max Strain, at Anterior Surface of Proximal Femur	Change in Strain Relative to Co−Cr	Specific Modulus Relative to Co−Cr
cobalt−chromium	7.67E−4	NA	1.0
titanium	9.41E−4	+23%	0.53
aluminum	1.05E−3	+37%	0.34
bone modulus	1.29E−3	+68%	0.07

Examining the strains in the interior of the proximal femur by plotting Von Mises strain on a longitudinal planar section through the femoral long axis provides a different view of the changes due to implant modulus reduction. See Figures 15 through 19. The results of comparing these sections are presented in Table 5.

Table 5. Maximum Strain for Different Implant Materials on Longitudinal Section of Proximal Femur on Surface of Interior Preparation Cut

Implant Material	Max Strain, on Plane Cut Through Proximal Femur	Change in Strain Relative to Co−Cr	Specific Modulus Relative to Co−Cr
cobalt−chromium	9.09E04	NA	1.0
titanium	1.15E−3	+27%	0.53
aluminum	1.32E−3	+45	0.34
bone modulus	1.77E−3	+94	0.07

The reduced stiffness implants had more of an effect on increasing strain closer to the proximal end (near the implant) than farther from the proximal end. In both cases, there were substantial increases in strain in the femur with the lower modulus metal implants, and a very large increase in strain in the femur for the implant with a modulus the same as bone. An increase in the local strain of 94% is a substantial change.

The intact femur section view (Figure 15) indicates that, for this load case, there is a lower strain in all areas of the proximal portion of the intact femur than in any of the complete hip arthroplasty femurs.

Figures 20 through 24 show a series of strain plots on cross sections through the femur perpendicular to the long axis. In addition, the implant surface strain has been plotted, primarily to provide a clear reference for the strain plot sections, but also to show the increasing strain in the implants as the modulus is reduced.

Figure 24 is a bit unusual, in that the implant appears to be missing some of the neck region. This is a display artifact caused by a limitation of the strain plotting software. To control the range of colors to the particular range of strain levels of interest, the maximum strain on the color bar is set to 2.0E−3 (strain is unitless; inch/inch or mm/mm). The strain plotting software does not plot strains that are higher than the maximum value selected on the color bar, and for the bone modulus implant, the strains in the neck region are high enough to be missing in the plot. The strain color bar scale was not changed so that Figures 20 through 24 would be directly comparable. The strains in the implant neck are not important to the primary subject of this study. It is clear that if an actual bone−modulus implant were to be designed, it would have head and neck region of a different geometry than the implant modeled here.

It is clear that there is a proportionate increase in the strain carried in the bone as the implant stiffness is decreased, as has been hypothesized. This study uses relatively high resolution models, which provide a clear verification of the trend. This set of models is detailed enough to report the detailed strain distributions through the femur for the load case used.

An interesting thing to note in Figures 20 through 24 is the visible differences in the strains on lowest two cross sections as the implant stiffness varies. At the cross section which is just at the tip of the implant, the strain distribution is unchanged over the range of implant stiffnesses, which covers a factor of 10 in stiffness. In contrast, the adjacent cross section, which is located only 20 mm up the femur toward the proximal end, shows noticeable increases in strain as the implant modulus decreases. The differences at this cross section between cobalt−chrome and titanium are difficult to distinguish, but the differences are clear for the aluminum and bone modulus implants. This appears to be related to the presence of the implant stem causing the strain inflection to move to beyond the tip of the implant stem. While the strain at the inflection point just beyond the tip of the stem does not seem to vary, the strains in the bone surrounding the stem do vary noticeably with implant stiffness.

The underlying phenomenon revealed in this series of plots is that the stiffer the implant, the shorter the portion of the stem that is active in carrying loads to the bone. In Figures 10 through 13 (longitudinal sections cut through the femur) the strain in the bone on the interior surface of the femur near the implant tip is extremely low for the cobalt−chromium alloy. The strain contour for 5.0E−4 intersects the medial exterior surface in almost exactly the same location for all four different implant stiffnesses, but this strain contour behaves quite differently on the interior of the bone. For the cobalt−chrome implant, the 5.0E4 strain contour is never broken and flows up the bone from the implant tip area, joining to the same strain contour in the proximal femur. For the titanium implant, the same 5.0E−4 contour ends at the interior surface roughly half way up the implant stem. For the aluminum implant, the same contour ends at the interior surface a bit more than one−third of the way up the stem. For the bone modulus implant, the 5.0E−4 strain contour ends at the interior surface about one−fourth of the way up the stem. Clearly, the less rigid implants distribute the loads

into a larger portion of the femur, increasing the local strain as that larger area of bone is required to carry a portion of the load. This increased strain could be expected to cause less bone to be resorbed over the life of the more flexible implant. The increased strain in the interior of the femur shown in Figures 16 through 19 and 21 through 24 should reduce internal bone resorption or possibly even promote addition bone growth. This could assist in maintaining fixation of the implant over a longer period, thus extending implant useful life.

Hard Cement Versus Soft Cement

The acrylic cement used to bond the implant into the prepared femur has a reported modulus of elasticity of 2,300 MPa. This cement was used in all the cases reported up to this point.

To evaluate the effects of cement stiffness on the strain distribution in the femur, a model was run with much stiffer cement and another was run with much more flexible cement. The stiffer cement has a modulus of elasticity of ten times the acrylic, or 23,000 MPa. The reduced stiffness cement has a modulus of elasticity of one−tenth the acrylic, or 230 MPa. The implant used in both cases was the baseline implant, the production cobalt−chromium alloy version.

No effort was made to relate the hard cement or the soft cement material properties to actual materials. This portion of this study was purely theoretical, to conceptually examine the effect of stiffer or more flexible cements. Since this is one of the available variables potentially available in the process of total hip arthroplasty, it should be studied. Actual cement materials that are stiffer or more flexible than current cements and compatible with the human body may be developed if the study indicates benefits relative to the current material.

Figures 25, 26, and 27 show longitudinal sections through the proximal femur with high modulus cement and low modulus cement, with the standard modulus cement in the center position (Figure 26, identical to Figure 16) for reference. All three models used the standard cobalt−chromium alloy implant.

The results indicate that for an implant with this geometry, increasing the cement stiffness substantially increases the strains near the preparation cut, close to where the implant flange rests on the preparation cut. More flexible cement dramatically reduces these highly localized strains. At the same time, the strains in the femur approximately 50 mm below the preparation cut are reduced with the stiff cement and increased with the flexible cement. The stiffest cement caused lower strains in the femur just beyond the implant tip, and the standard cement and more flexible cement caused increased strain near the implant tip. Basically, the more flexible cement seemed to distribute the loads into the femur lower on the femur, and the more rigid cement seemed to keep the maximum strain closer to the proximal end. These results are summarized in Table 6.

Table 6. Comparison of Effects on Strain Distribution of Cement Stiffness Changes

Cement	Strain Changes Near Implant Flange	Strain Changes 50mm From Prep Cut	Strain Changes Just Beyond Implant Tip
stiffer	increased	decreased	decreased

more flexible	decreased	increased	increased

Partner Contribution

Brandon Research team members provided the whole of the medical basis and virtually all the geometry, boundary conditions, and material properties for the simulation work. Brandon Research consultant, Dr. Robertson, and his technical assistants carried out the creation of the femur medical CAD surface model and implant CAD model. Brandon Research carried out the literature survey, which identified loading conditions that were appropriate and previously used by other researchers investigating similar situations and conditions of the human femur. The Brandon Research medical doctors provided instructions on how the implant was to be mated to the femur, which included implant sizing, femur head removal guidelines, femur interior bone removal guidelines, implant placement, and cement application. The material properties for the bone, implant, and the cement were researched and provided by the Brandon Research team.

Financial

The original budget from the DOE was for $50,000. Due to technical difficulties which are covered briefly in the Technical section of this report and competition for the Principal Investigator s time by high−priority DOE production work, the project was extended beyond the originally planned completion date and additional funds approved. This additional funding represented $15,000 above the original budget.

Property and Proprietary Information

There was no proprietary information used or created during this project.

Acknowledgment

The Principal Investigator would like to thank the U. S. Department of Energy for the support of this project. This funding has made it possible to apply some of the most capable mechanical engineering simulation hardware and software available today to advance the study of the solid modeling of biological shapes and the details of the interaction between man−made implants and the original bone.

References

1D. R. Carter, T. E. Orr, and D. P. Fyhrie, "Relationships Between Loading History and Femoral Cancellous Bone Architecture," *Journal of Biomechanics*, Vol. 22, No 3, pp 231−244, 1989.

2James A. St. Ville, John A. Ecker, James M. Winget, Meri H. Berghaur, *The Anatomy of Mid−Thigh Pain After Total Hip Arthroplasty,* published by Institute for Bone and Joint Disorders,
3320 N. 2nd St., Phoenix, AZ 85012.

Bibliography

"Relationships Between Loading History and Femoral Cancellous Bone Architecture,"
D. R. Carter, T. E. Orr, D. P. Fyhrie, *Journal of Biomechanics*, Vol. 22, No. 3, pp. 231−244,1989.

The Anatomy of Mid−Thigh Pain After Total Hip Arthroplasty, James A. St. Ville, MD, MS;
John A. Ecker, BSME; James M. Winget, Ph.D.; Meri H. Berghauer, BA

published by: James A. St. Ville, MD

Institute for Bone & Joint Disorders

3320 N. 2nd St.

Phoenix, AZ 85012

"Cementless Implant Composition and Femoral Stress," R. S. Namba, MD; J. H. Keyak, Ph.D.;
A. S. Kim, MS; L. P. Vu, MD; H. B. Skinner, MD, Ph.D.; *Clinical Orthopaedics and RelatedResearch*,
Number 347, pp. 261−267, Lippincott−Raven Publishers, 1998.

ABAQUS/Standard User s Manual, Version 5.7, Hibbit, Karlsson & Sorensen, Pawtucket, RI.

Military Handbook 5F, Metallic Materials and Elements for Aerospace Vehicle Structures, 1990, U. S. Department of Defense, FSC 1560.

Figures

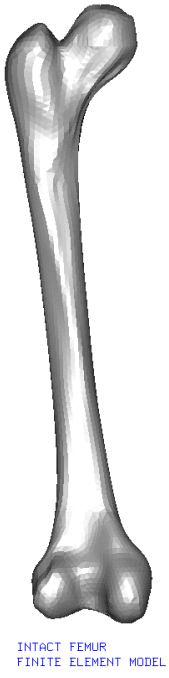

Fig. 1a. *Shaded image of finite element model of left femur, anterior*

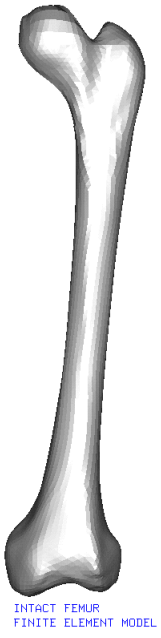

Fig 1b. *Shaded image of finite element model, posterior*

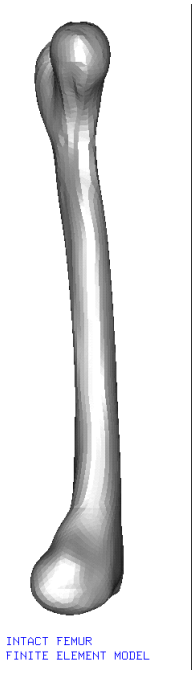

Fig 1c. *Shaded image of finite element model, medial*

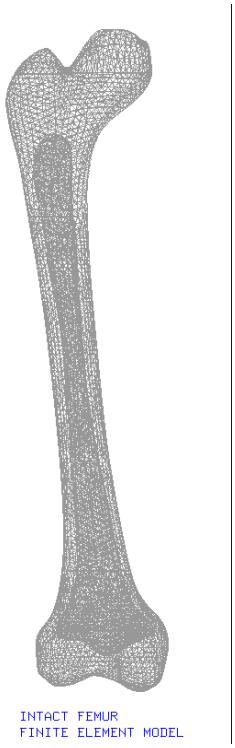

Figure 2a. *Overall view of finite element model, intact femur*

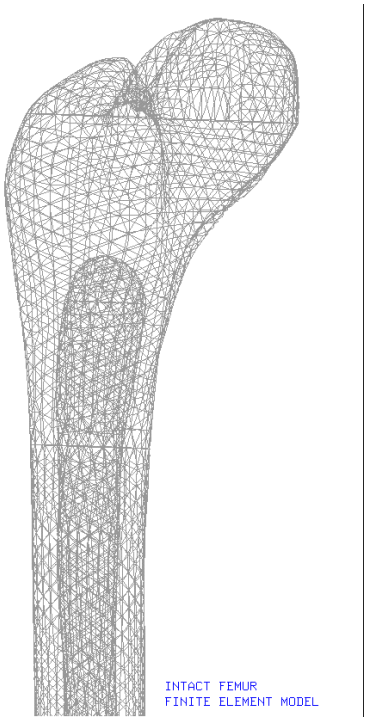

Figure 2b. *Proximal detail of finite element model, intact femur*

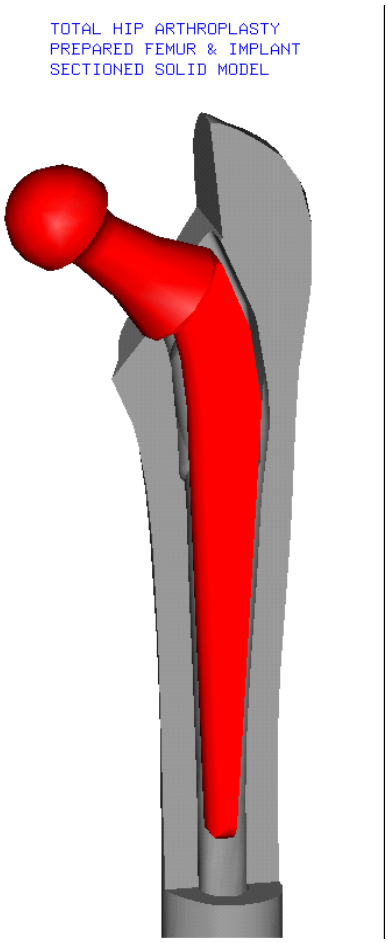

Figure 3. *Section view of implant located in prepared femur,without cement*

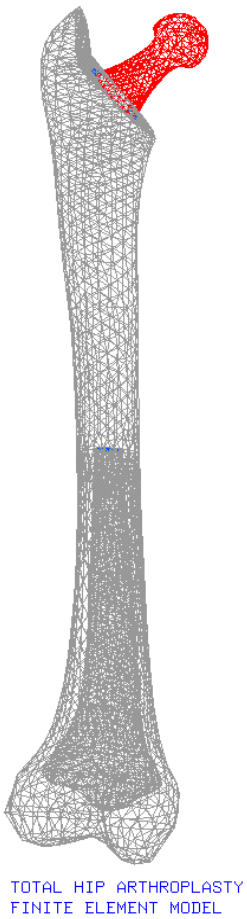

Figure 4a. *Finite element* model of femur after total hip arthroplasty

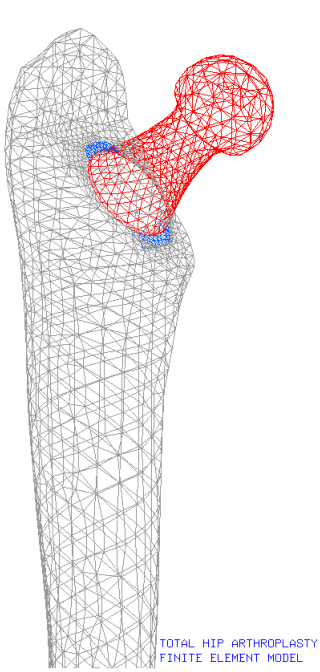

Figure 4b. *Proximal end* details of FE model

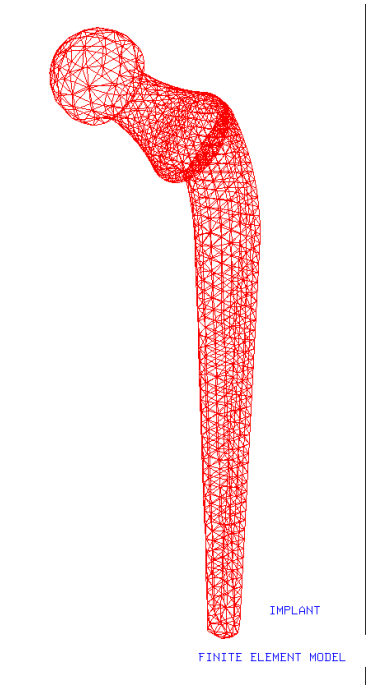

Figure 5. *Finite element model of implant device*

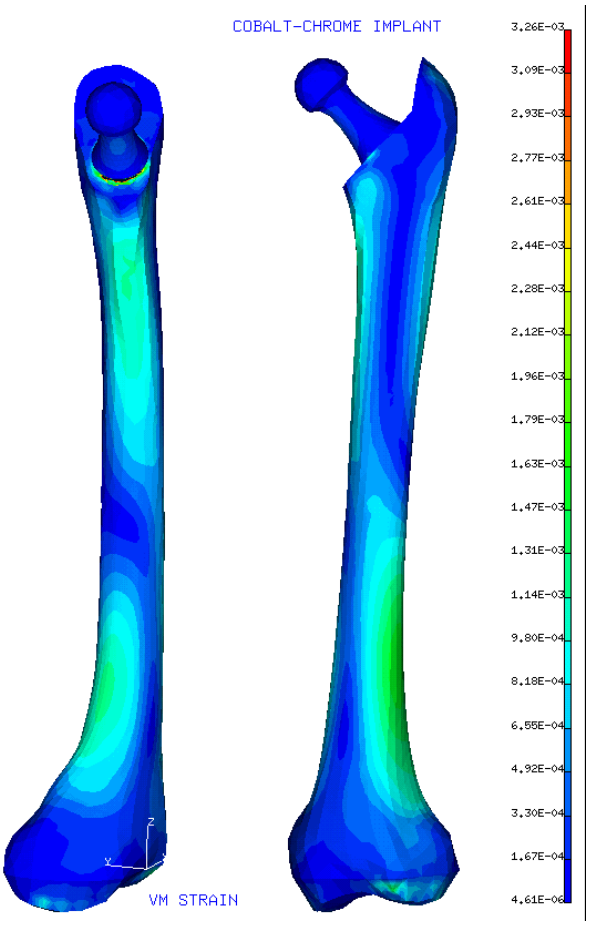

Figure 6. *Contour plot of Von Mises strain* on exterior surface of **intact femur**

Figure 7. *Contour plot of Von Mises strain* on exterior surface of implanted femur − with **cobalt−chromium implant**

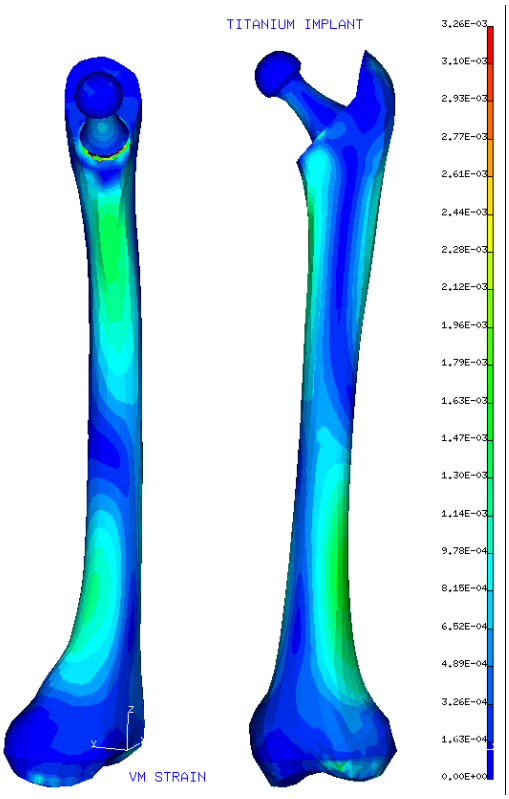

Figure 8. *Contour plot of Von Mises strain with* ***titanium implant***

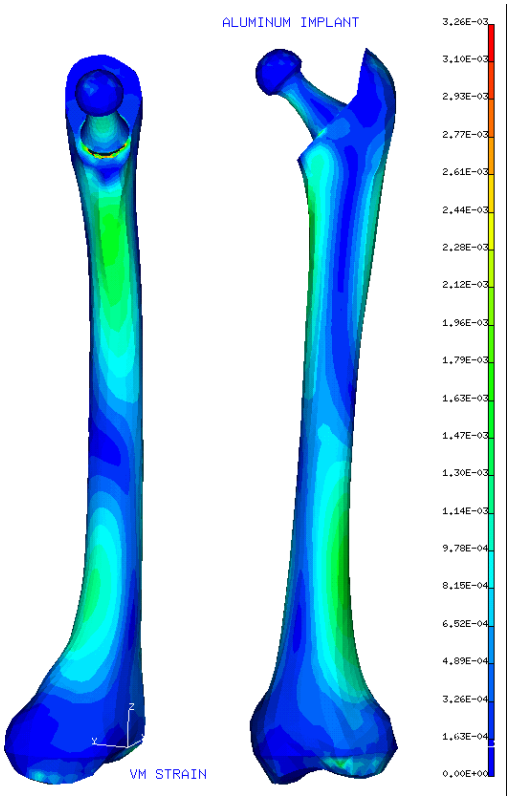

Figure 9. *Contour plot of Von Mises strain with* aluminum implant

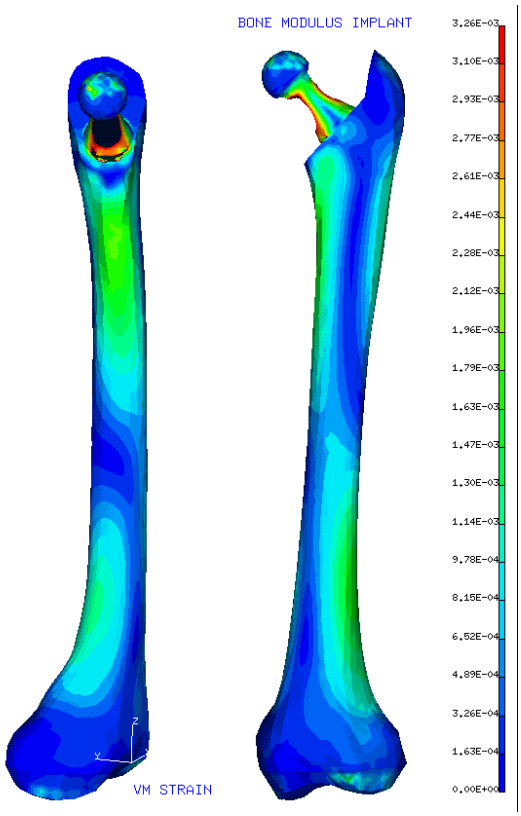

Figure 10. *Contour plot of Von Mises* strain with **bone modulus implant**

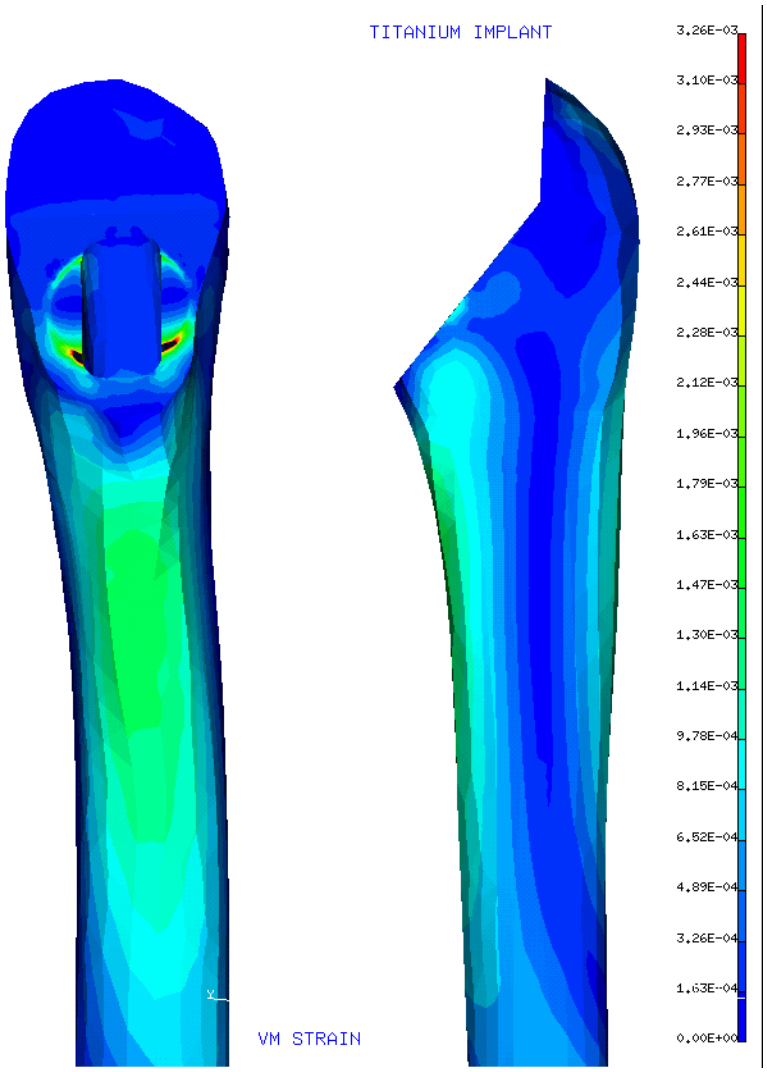

Figure 11. *Strain plot on proximal end of femur with* cobalt−chromium implant

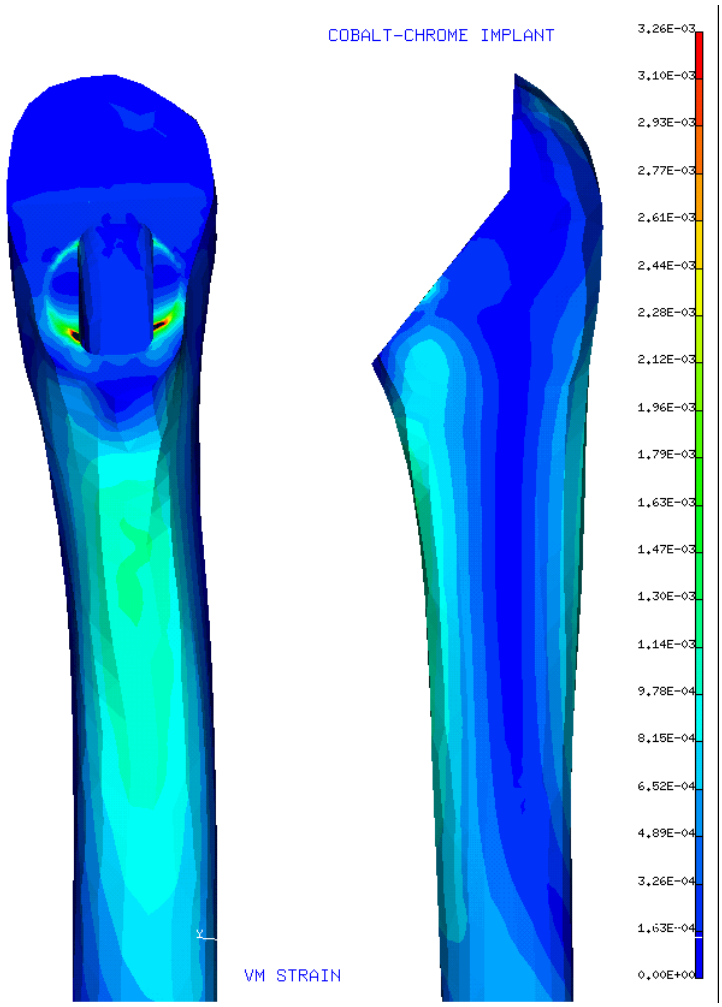

Figure 12. *Strain plot on proximal end of femur with* titanium implant

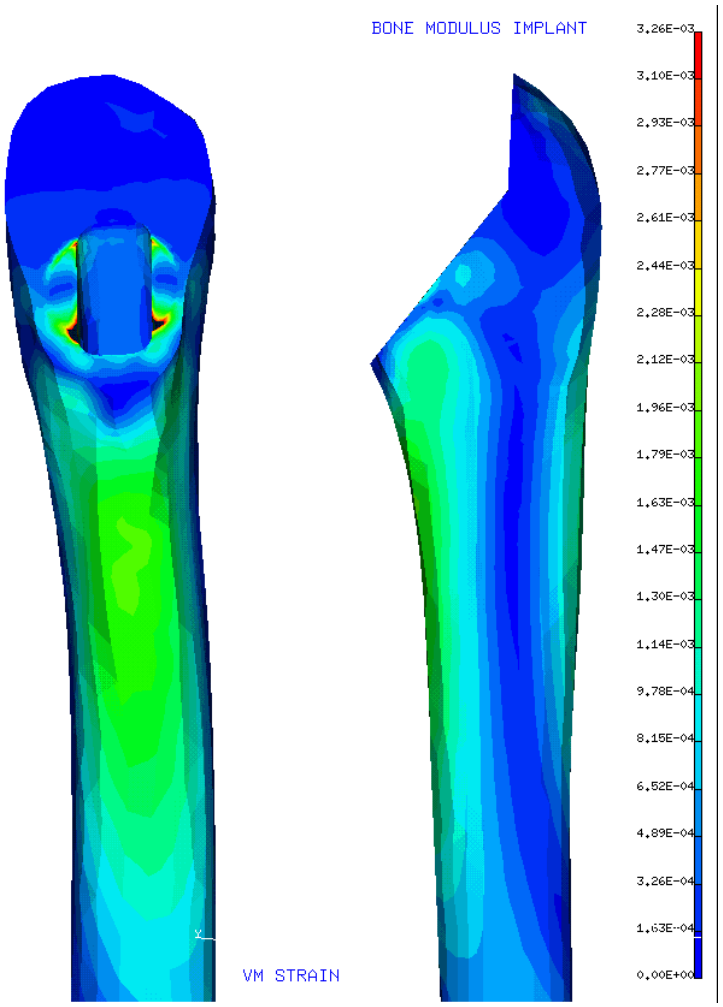

Figure 13. *Strain plot on proximal end of femur* with **aluminum implant**

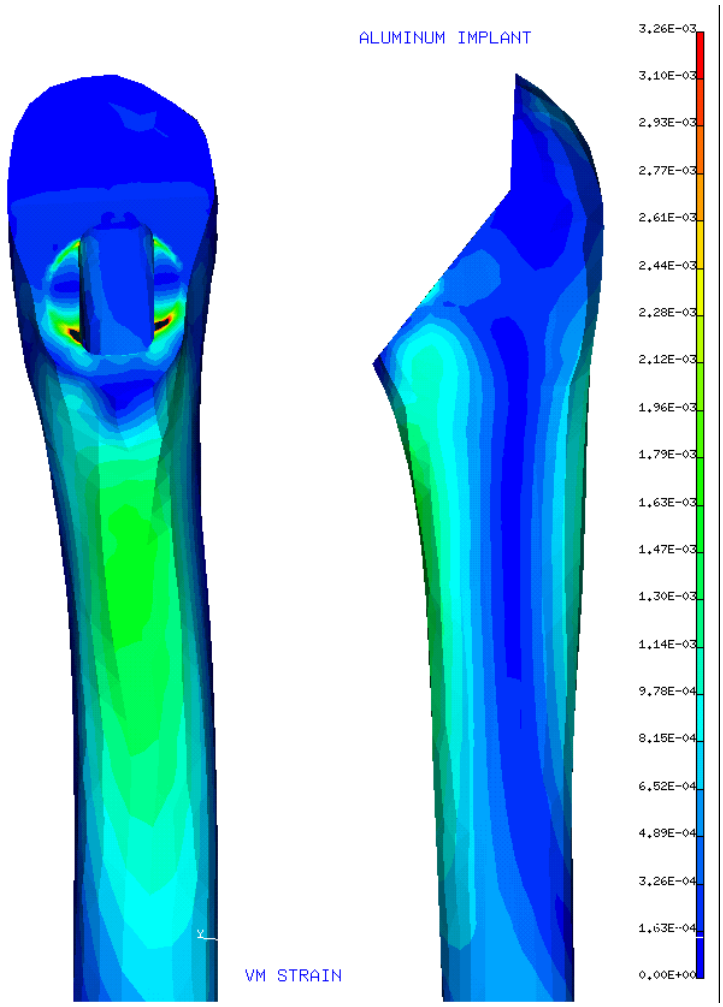

Figure 14. *Strain plot on proximal end of femur* with **bone modulus implant**

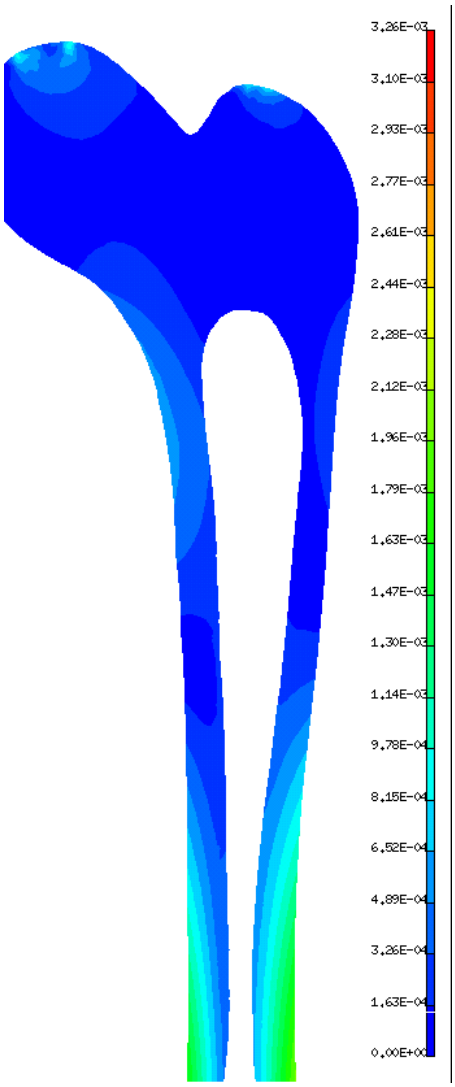

Figure 15. *Strain plot on* longitudinal cutting plane through intact proximal femur

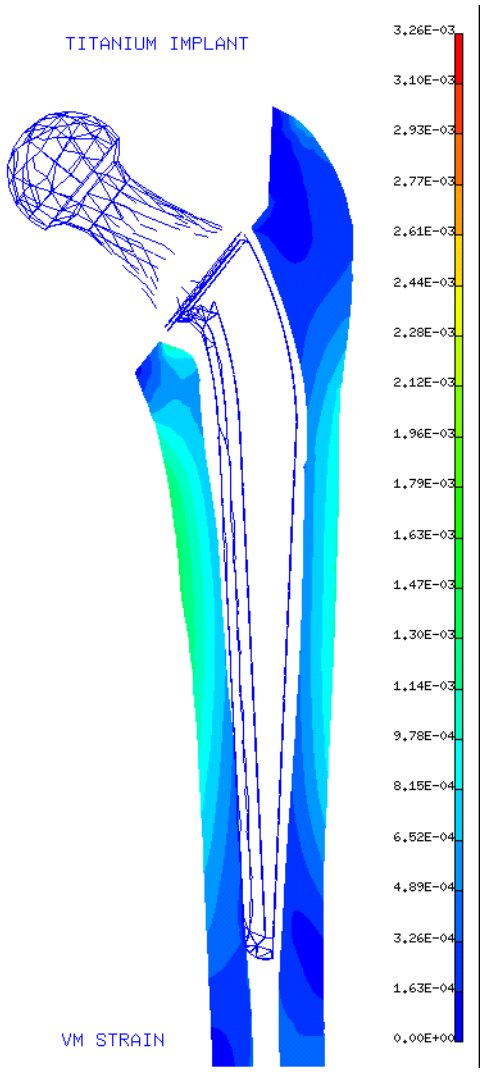

Figure 16. *Strain plot on longitudinal plane* cut through proximal femur, **cobalt−chromium** implant

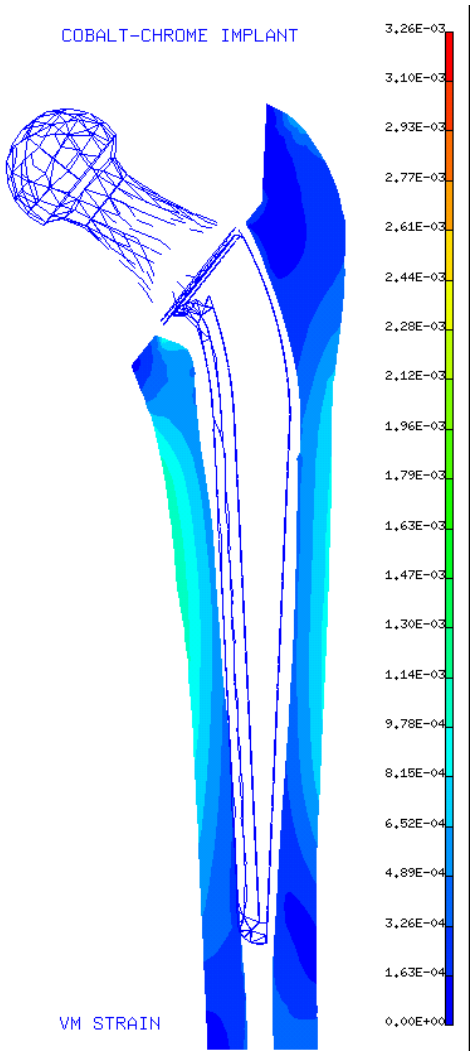

Figure 17. *Strain plot on longitudinal plane cut through proximal femur,* ***titanium implant***

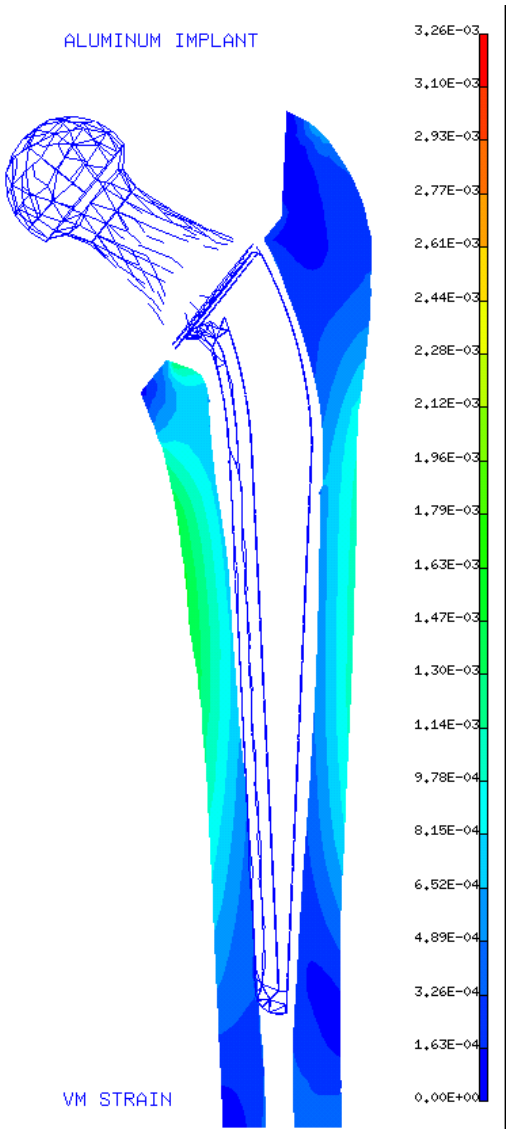

Figure 18. *Strain plot on longitudinal plane cut* through proximal femur, **aluminum implant**

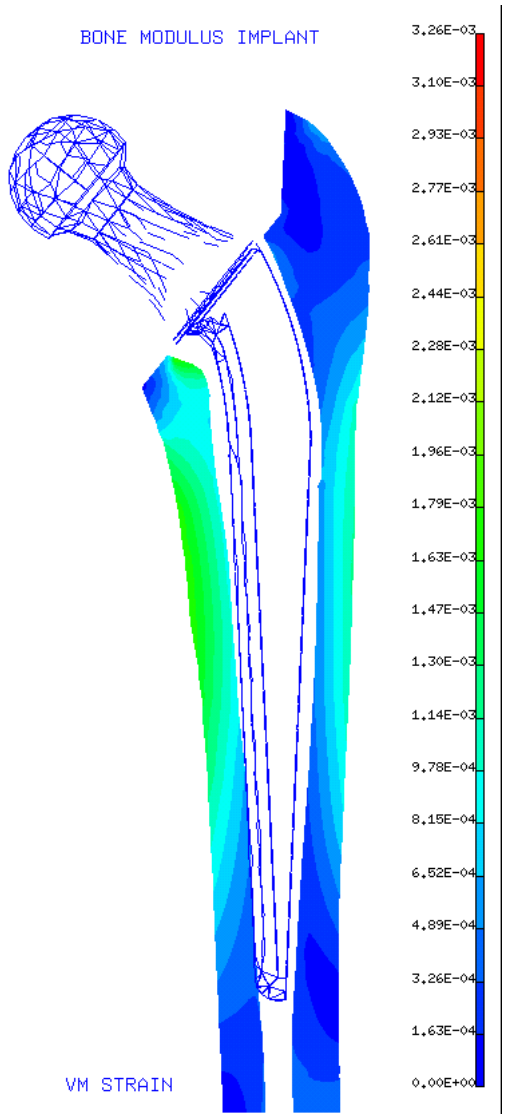

Figure 19. *Strain plot on longitudinal plane cut* through proximal femur, **bone modulus implant**

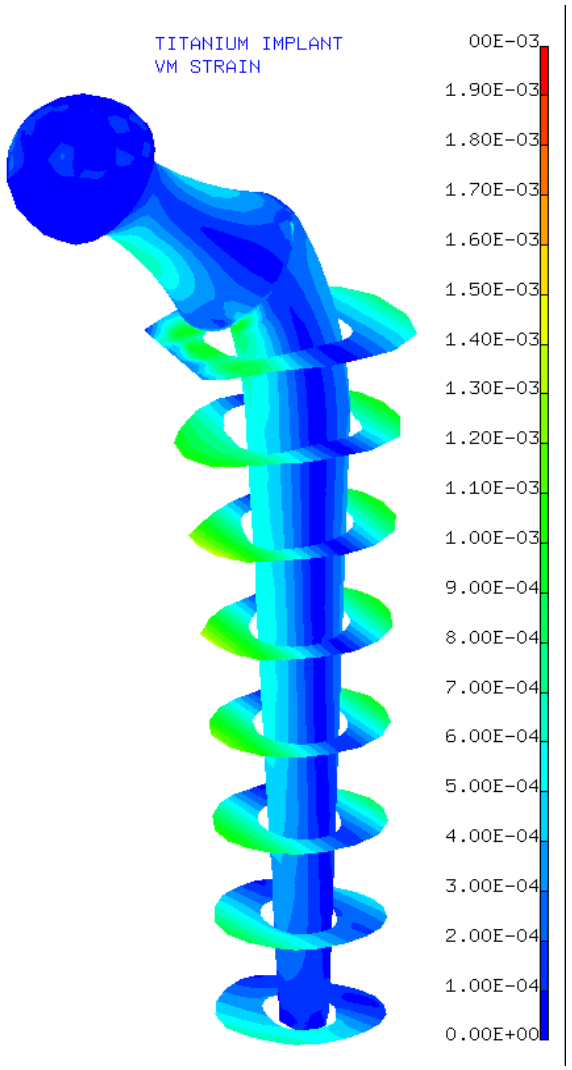

Figure 20. *Strain plots on* sections of intact femur

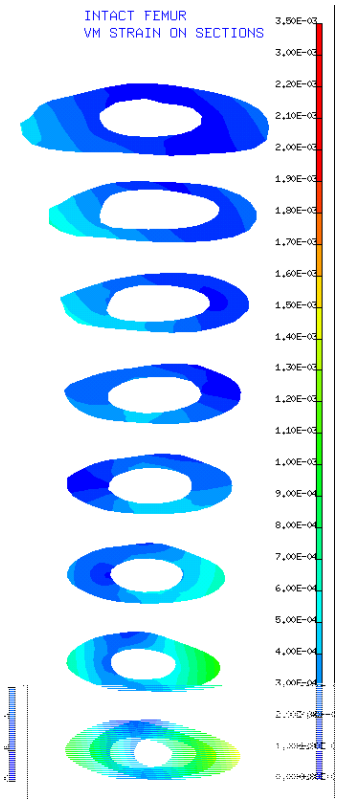

Figure 21. *Strain plots on sections of femur*, with **cobalt−chromium implant**

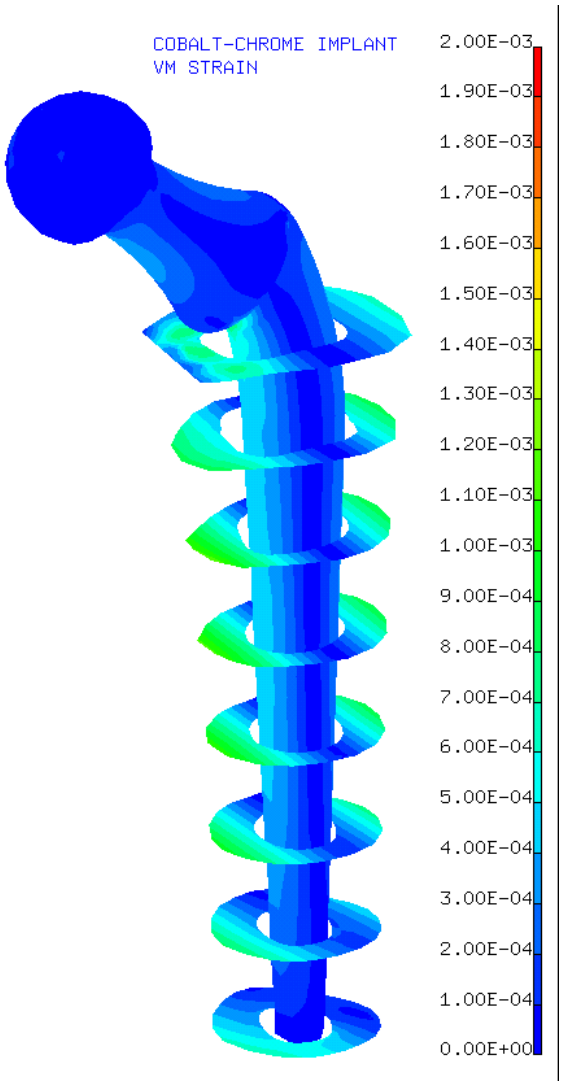

Figure 22. *Strain plots on sections of femur, with* titanium implant

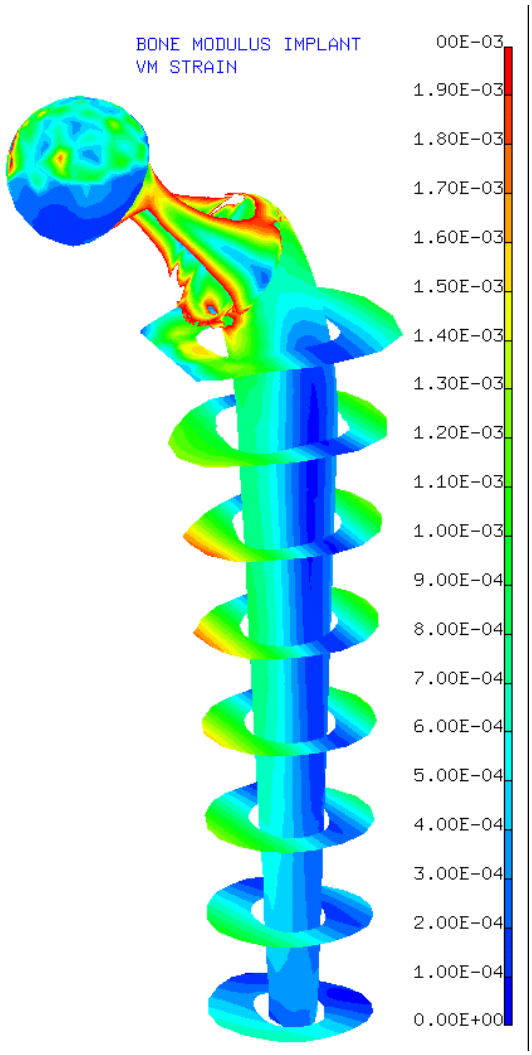

Figure 23. *Strain plots on sections of femur, with* aluminum implant

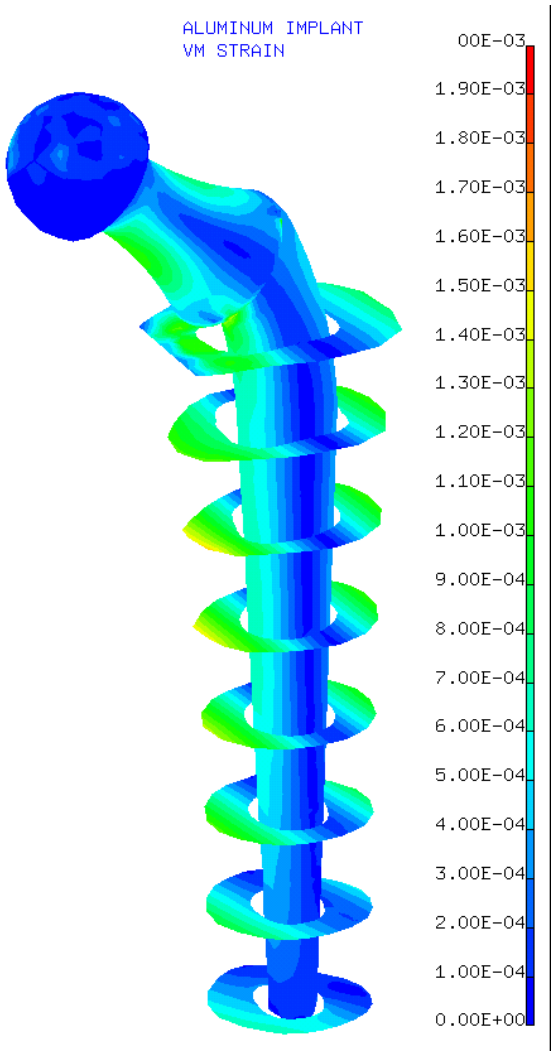

Figure 24. *Strain plots on sections of femur, with* bone modulus implant

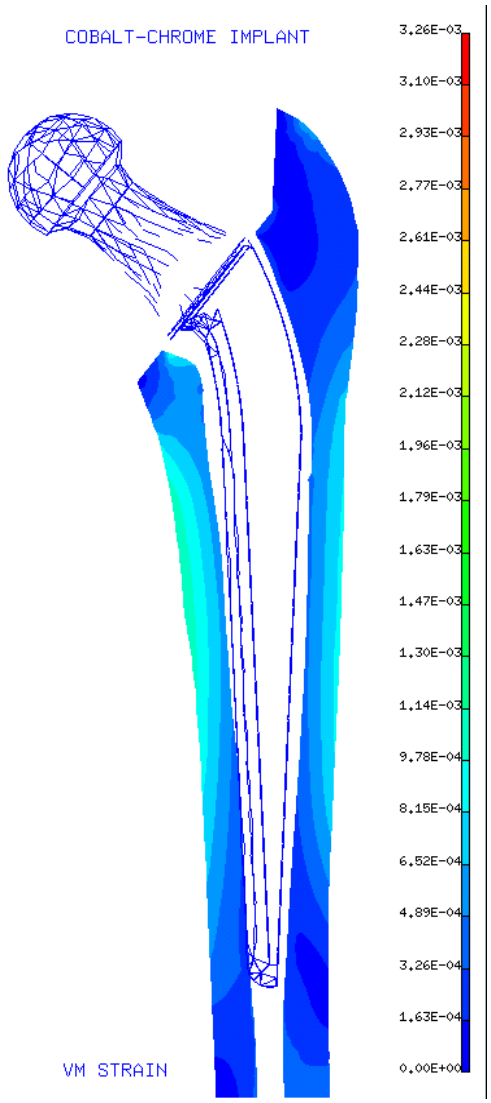

Figure 25. *Strain plots on longitudinal section* through proximal femur, **high modulus cement** with cobalt−chromium implant

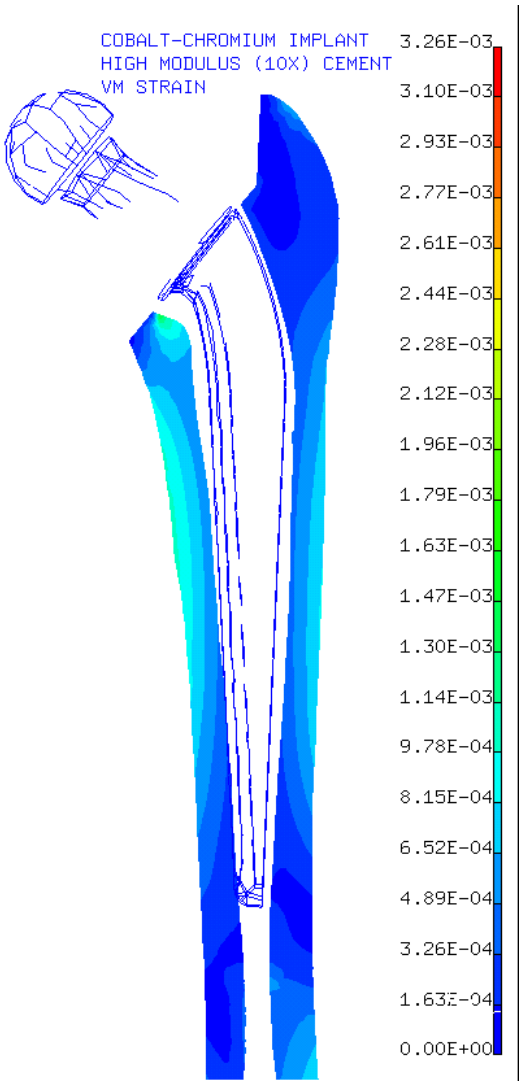

Figure 26. *Strain plots on longitudinal section* through proximal femur, **standard cement** with cobalt−chromium implant

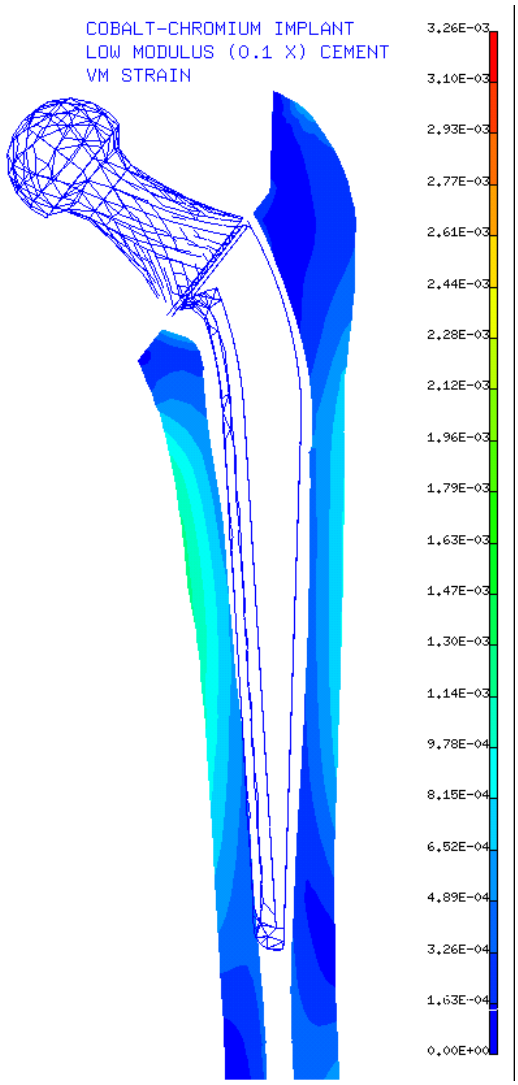

Figure 27. *Strain plots on longitudinal section* through proximal femur, **low modulus cement** with cobalt−chromium implant